Earth and Planetary Science Letters 597 (2022) 117817

Contents lists available at ScienceDirect

Earth and Planetary Science Letters

www.elsevier.com/locate/epsl

3D-simulation of lunar megaregolith evolution: Quantitative constraints on spatial variation and size of fragment

Tiantian Liu [a,*], Kai Wünnemann [a,b], Greg Michael [b]

[a] Museum für Naturkunde, Leibniz Institute for Evolution and Biodiversity Science, 10115 Berlin, Germany
[b] Freie Universität Berlin, Malteserstr., 74-100, 12249 Berlin, Germany

ARTICLE INFO

Article history:
Received 9 November 2021
Received in revised form 6 September 2022
Accepted 8 September 2022
Available online 20 September 2022
Editor: W.B. McKinnon

Dataset link: https://doi.org/10.35003/EBULMM

Keywords:
Moon
early bombardment
megaregolith
cumulative fragmentation
impact processes
Monte Carlo simulation

ABSTRACT

The early impact bombardment extensively fractured the lunar crust resulting in the formation of the so-called megaregolith. Previous estimates of megaregolith distribution vary significantly with respect to the vertical extent and the size-frequency distribution of fragments was rarely studied. We built a spatially resolved numerical model to simulate the process of cumulative impact fragmentation, aiming to backtrack the megaregolith evolution history and to constrain its fragment distribution. The results highlight the pivotal role of basin-forming events on the megaregolith formation. Especially the South-Pole Aitken (SPA) impact established the initial megaregolith structure which remained distinct after 0.5 Ga subsequent fragmentation. At 3.8 Ga, the megaregolith displays substantial lateral variation and layering: the highly fractured upper layer of ~2.5 km is dominated by meter-scale fragments; the disturbed lower layer deeper than tens of kilometers is mainly consisting of kilometer-scale fragments; the transition zone >5 km contains fragments of various size scales.

1. Introduction

Numerous large impacts occurred during the early bombardment period, shattering and fracturing the lunar crust, producing a globally fragmented layer known as megaregolith (Hartmann, 1973, 2003, 2019; Hartmann and Morbidelli, 2020; Hörz et al., 1991). Understanding how the megaregolith evolved is important for understanding the lunar thermal evolution history since the crust became more fractured with the cumulative impact cratering influencing the thermal conductivity (Warren and Rasmussen, 1987). In addition, due to the insulation effect, the presence of megaregolith affects the estimate of the bulk content of Uranium and hence the overall composition of the Moon (Warren and Rasmussen, 1987). The petrophysical properties of megaregolith, such as porosity and related strength, significantly differ from pristine rocks resulting in variations in the relationship between impact crater size and impact energy (Marchi et al., 2011).

The thickness of the megaregolith layer was investigated based on ejecta estimates (Housen et al., 1983; McGetchin et al., 1973; Petro and Pieters, 2008; Pike, 1974), or on radar and optical data (Blanchette-Guertin et al., 2012; Thompson et al., 2009). The estimates were, however, highly diverse ranging from a few hundreds of meters up to tens of kilometers. In addition, due to the specific regional bombardment history of a certain area, the degree of fragmentation of the crust varies regionally and the megaregolith is expected to possess substantial lateral variability (Hörz et al., 1991). However, previous studies mostly presented estimates of the global average and some focused only on the near-surface fragmentation (Hörz, 1977; Rolf et al., 2017). Wiggins et al. (2019) recently investigated the deep-seated fragmentation by single impact events, but the influence of subsequent impacts on those fragments remains to be studied.

The fragment size distribution at different depths in the megaregolith has been little investigated and lunar observations merely allow some qualitative constraints (Besserer et al., 2014; Elder et al., 2019; Wieczorek et al., 2013). Improved quantitative constraints of the megaregolith distribution can provide a reference framework for developing sampling strategies. The lunar surface is covered with fine-grained regolith, and surface rocks even of meter-scale are typically eroded within a few hundred Ma. To collect lunar rock samples, we are dependent on excavation processes in the megaregolith (Hartmann and Morbidelli, 2020). The distribution of fragment size is also essential for the interpretation of remote sensing data. For example, the bright craters in Earth-

* Corresponding author.
E-mail address: Tiantian.Liu@mfn.berlin (T. Liu).

https://doi.org/10.1016/j.epsl.2022.117817

based radar images are thought to be related to the excavation of megaregolith fragments (Thompson et al., 2009).

Here we built a spatially resolved numerical model to investigate the consequences of the cumulative impact fragmentation by embedding the impact fragmentation process into our previous impact mixing model (Liu et al., 2020a). We define the megaregolith as the accumulated fragments that have resulted from the impact fragmentation process during the heavy bombardment period when giant basin-forming events occurred. We aim to quantitatively constrain both the vertical and lateral structure of the megaregolith and trace back its evolution history. In section 2, the model mechanism is described. Using this model, we estimate the spatial variation and fragment size of megaregolith (section 3). In section 4, the leading factors concerning the quantitative fragmentation process on the megaregolith formation are discussed. With the knowledge of model sensitivity, we finally present the evolution paths of the megaregolith.

2. Methods

Our impact mixing model was designed to trace the evolution of different target components with long-term bombardment (Liu et al., 2021, 2020a, 2020b). By tracing different-sized fragments caused by the impact cratering, we use this model to investigate the cumulative fragmentation process. In this section, we describe the essential components of the model. More detailed explanations are contained in the supporting information.

We use the Monte Carlo method to simulate the cumulative impact cratering considering a monotonically decaying impact flux (Neukum, 1983). Craters larger than 20 km are considered and the size-frequency distribution of generated craters follows the Neukum Production Function (NPF, Neukum, 1983). The large-scale basin events are treated separately and we simulate their occurrence according to a table of actual lunar basins (Fig. 1a). The model starts (t_0) slightly earlier than the estimated formation time of the ancient South Pole–Aitken basin (SPA), and ends after the occurrence of the youngest basin (3.8 Ga, Orientale basin; Fassett et al., 2012). There are 18767 impact events in total.

We model the impact fragmentation process after the solidification of the lunar magma ocean, or at least after the late solidification stage of the lunar magma ocean stage. All impacts form in a solid target and none penetrate as far as the magma ocean. At the model starting time, t_0, we assume the impact target as a solid sphere with a radius of the Moon and no lunar internal structure is considered. The initial surface is then fractured by numerous impact events that occur randomly over the surface (except for the basin-forming events). Each impact event damages the crust surrounding the impact site and generates different-sized fragments. Fragmented materials are partially expelled from the crater forming an ejecta layer in the vicinity of the crater (**allochthonous fragments**) and partially displaced and remain below the crater (**autochthonous/parauthochtonous fragments**). We assume that megaregolith is mostly characterized by large fragments and, thus, consider only fragments >1 m in diameter in our model.

The size-frequency distribution of ejected fragments has been extensively analyzed for laboratory-scale impact craters, nuclear explosion craters, and terrestrial and lunar impact craters, and rock fragmentation observations (Bart and Melosh, 2010; Moore, 1970; Watkins et al., 2019). A power-law relationship is commonly used to fit the fragment size-frequency distribution: $N(m) = C_1 m^{-b}$, where $N(m)$ is the cumulative number $N(m)$ of fragments with mass of $\geq m$, and C_1 is a constant. Both experiments and observations of lunar craters (Bart and Melosh, 2010; Buhl et al., 2014; Watkins et al., 2019) reveal b fluctuating between ~0.7 and ~1.8. The median value of 1.2 is taken for simulations. Larger fragments occur closer to the crater rim (Bart and Melosh, 2010; Krishna and Kumar, 2016; Moore, 1970), and the size of the largest fragments is related to the crater diameter: $l_{E0} = C_2 D^{2/3}$, where C_2 is a constant with a value ranging from ~0.1 to ~0.3. We take the lower limit in our simulations. To simulate fragment distribution in ejecta, while ensuring the general thickness distribution (equation 1 in the supplementary file), we assume large fragments are located close to the rim and smaller fragments dominate the distal deposit. Although ejecta at any given range is a mixture of different-sized rocks, the decreasing average fragment size with the increasing distance from the crater center has been verified in numerous impact experiments (Melosh, 1989; chapter 6).

The size of autochthonous fragments below the crater floor is poorly known. Deep drilling (e.g. Puchez Katunki, Ivanov et al., 1996) and field studies at exposed central peaks of terrestrial craters (e.g. Upheaval Dome and Jebel Waqf as Suwwan crater, Kenkmann et al., 2010, 2006) provide some first order estimates of the size of fragments or megablocks. The fragment size distribution underneath craters is also crucial for the so-called acoustic fluidization (AF) model proposed by Melosh (1979). The model explains complex crater formation at the observed threshold crater diameter which requires a temporary significant reduction of strength to explain the weak behavior of rocks during crater formation and transient crater collapse (Melosh and Ivanov, 1999). Systematic modeling studies of crater morphometry compared with the observed lunar crater record revealed a relationship between crater size and the average fragment size (Wünnemann and Ivanov, 2003). In addition, as revealed by both the terrestrial observation and numerical modeling (Kenkmann et al., 2006; Wiggins et al., 2019), the size of deeper autochthonous fragments (l_B) is increasing with the distance from the crater floor (r_B). Using a linear relationship between l_B and r_B, we determine $l_B = l_{B0} + C_3 r_B$, where l_{B0} is the size of autochthonous fragments close to the crater floor and is determined by the AF model; C_3 is constant and taken to be 0.4 (Kenkmann et al., 2006).

Later impact events occur on the fractured target and break the fragments into smaller pieces. Their excavated fragments are further smashed and the produced allochthonous fragments follow the $N(m)$ distribution. The fragments underneath the impact occurrence region could also be broken up by autochthonous fragmentation. In this model, we consider this to happen if the determined l_B of a certain depth is smaller than the size of existing fragments.

The proposed simplified parametrizations are derived from numerical modeling and observations of lunar and terrestrial craters and come with large uncertainties. By varying the input parameters regarding the distribution of allochthonous and autochthonous fragments, this study provides clues on key parameters affecting the megaregolith formation (section 4). In addition, after the formation of the transient crater, the subsequent modification including the slumping of the crater walls and stepped terrace formation, results in a complex intermixture of fragments inside the crater depression. The modification process resulting in some change of the size-frequency distribution of fragments is not taken into consideration here.

3. Distribution of megaregolith

To indicate the general degree of fragmentation and the big picture of megaregolith, we calculate the volume-weighted average fragment size over the surface: $l_V = \frac{\sum_{i=0}^{14} l_i \times V_i}{\sum_{i=0}^{14} V_i}$ (l_i is the size of fragments and V_i is the volume of fragments with size l_i), where the smaller values indicate more abundant small fragments.

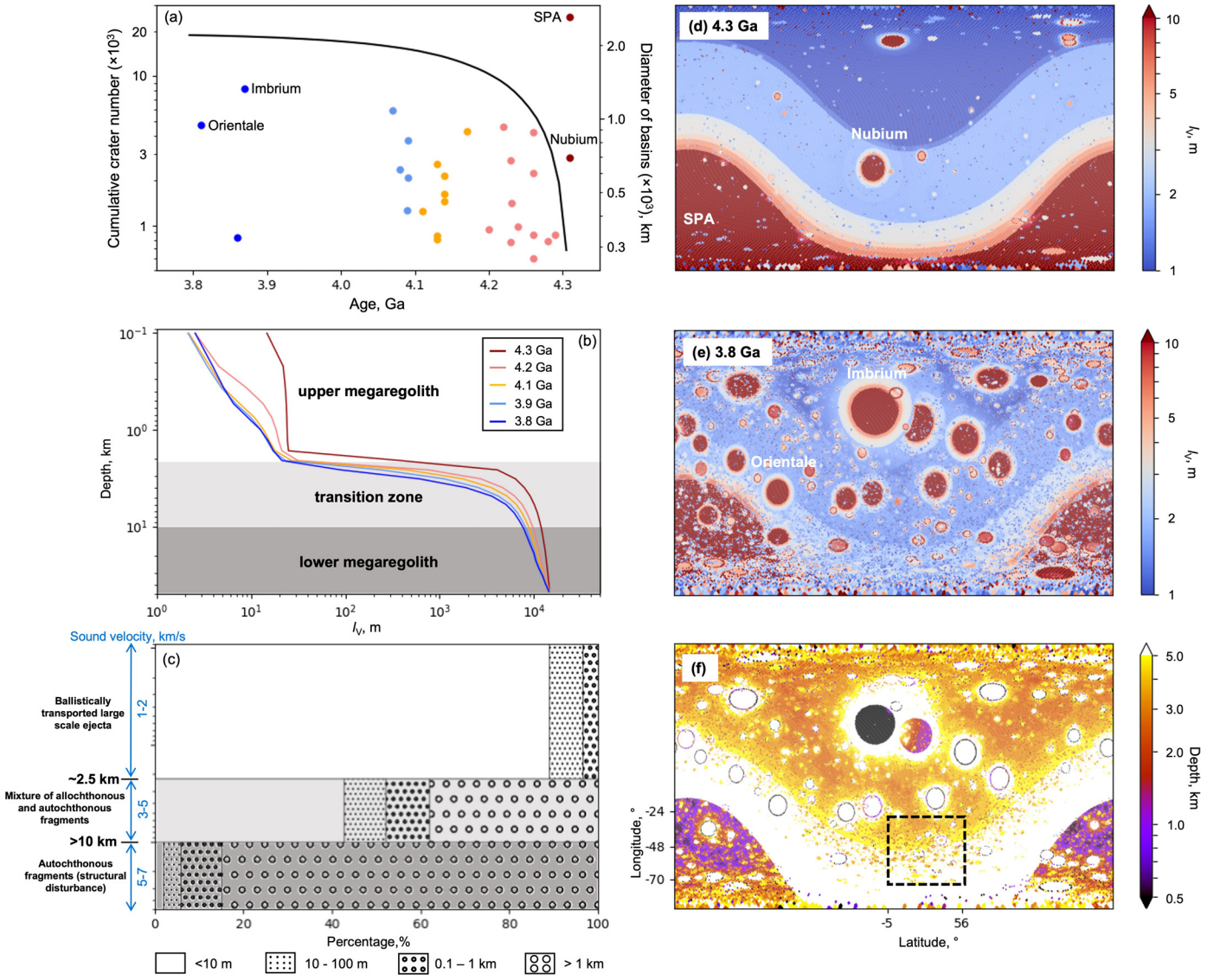

Fig. 1. (a) Cumulative distribution of craters >20 km (left y-axis) and the size of considered basin-forming events (right y-axis), where the basin age is taken from Orgel et al. (2018). (b) Evolving distribution of statistical fragment size l_V over the global surface with depth. $l_V = \frac{\sum_{i=0}^{14} l_i \times V_i}{\sum_{i=0}^{14} V_i}$ (l_i is the size of fragments and V_i is the volume of fragments with size l_i) is the volume-weighted average fragment size over the surface. (c) Contribution of various-scale fragments at different depths at 3.8 Ga. In (b) and (c), white, dark gray, and light gray indicate the upper megaregolith, lower megaregolith, and a transition zone in between. (d-e) Spatial variation of fragmentation degree of the near-surface megaregolith (the top 2 km) at 4.3 and 3.8 Ga, respectively. (f) Spatial variation of depth where fragments > 100 m become abundant with a fraction >0.5 (i.e., l_V>50 m) at 3.8 Ga. The dashed rectangle outlines the study area of radar-bright craters in Thompson et al. (2009) (Fig. S3). (For interpretation of the colors in the figure(s), the reader is referred to the web version of this article.)

3.1. Vertical structure

The megaregolith displays distinct layering: an upper megaregolith that mainly consists of ejected fragments with smaller sizes and a thickness of ~2.5 km; a lower megaregolith that mainly contains autochthonous fragments beyond 10 km depth. In between, there is no distinct boundary but a transition zone with a thickness of >5 km where allochthonous and autochthonous fragments are mixed. Our model-derived major source of the upper megaregolith being ejected fragments is consistent with the modelings of surface overturn depths and ejecta blanket thicknesses that have consistently pointed to an accumulative ejecta deposit in the near-surface about 1–3 km in thickness (Hartmann, 2019; Hiesinger, 2006). Recently, by using the Gravity Recovery and Interior Laboratory (GRAIL) gravity data, Izquierdo et al. (2021) characterized the porosity structure of the lunar upper crust, where they found a discrete change in porosity. This discrete change was proposed to reveal the boundary between the upper layer of the basin ejecta deposit and the deeper less damaged crust. Due to the sensitivity to the considered mean crustal density value, their estimated depth of this porosity change varies from 2.6 to 7.6 km. Our estimated thickness of the upper megaregolith falls in this range. The lower megaregolith mainly caused by the autochthonous impact fracturing is in line with the recent modeling work for dynamic fragmentation that concluded that impact craters 10's of kilometers in diameter can produce in-place fragments to a depth of ~20 km (Wiggins et al., 2019).

In the upper megaregolith, ~85% fragments by volume are in meter-scale. Due to the higher probability of being smashed by subsequent impacts, the shallower layer contains more small fragments than the lower, where the top 500 m contains >95% fragments in meter-scale. In the lower megaregolith, the disturbed deep crust consists of large-scale fragments, and >80% are in kilometer-scale. In the transition zone, ~40% fragments are in

kilometer-scale, and the fractions of fragments in the tens of meter- and hundreds of meter-scale are comparable.

Both the lunar seismic and gravity observations are in line with our predicted structure of megaregolith. Seismic measurements can distinguish between solid and fragmented rock. The seismic profiling of the lunar crust reveals an increase of the p-wave velocity with depth (Fig. 1c): the lower velocity in the top ∼2.5 km, a five times higher velocity deeper than 10 km, and an intermediate velocity in between. The impact fracturing causes a porous crust. The models of the interior structure based on the GRAIL gravity data revealed a high porosity in the upper few kilometers (12%), a four times lower porosity at the depth of 20 km, and a medium porosity at the depth of 10 km (Besserer et al., 2014; Wieczorek et al., 2013). Note that at the greater depths overburden pressure reduces and eventually inhibit fragmentation. In addition, due to the higher temperature at greater depths, thermal annealing of fragments (viscous deformation at elevated temperatures; Wieczorek et al., 2013) would weld the fracture, and the minimum depth of such process was estimated to be ∼40 km. But at this depth, this process does not have a significant effect on our modeling results since there is only very little material excavated from this depth. The timescale of such processes is basically unknown. We, therefore, do not take temperature-pressure long-term "healing processes" of a fractured crust into account here.

3.2. Spatial variation

At 4.3 Ga, soon after the SPA event, the lunar surface was covered with a layer of fractured rocks ejected upon the formation of SPA (Fig. 1d). Large fragments were distributed inside and near the SPA rim while distal regions were covered with smaller debris. Subsequent impacts that could not penetrate to the underlying less-damaged crust comminuted the fragments produced by the SPA impact, enriching the small fragments in the near-surface. Only large-scale impacts, especially the basin-forming events that did penetrate the SPA ejecta and excavate the less fractured bedrock, added some larger fragments to the near-surface (e.g., Nubium basin). After all the basins were formed at 3.8 Ga (Fig. 1e), due to the stochastic nature of the impacts, the megaregolith displays substantial lateral variability, being consistent with the modeling results of Hartmann (2019). Near the crater rims, larger fragments are pervasive. The abundance of these proximal, big fragments was gradually diluted by the mixing of smaller fragments entrained in the ejecta of later impacts, but the big fragments volumetrically remain predominant unless subsequent impacts occurred directly on them. Since no process that might heal fractures (e.g., recrystallization and recompaction; Hörz et al., 1991) is considered, the degree of fragmentation of some regional areas could be over estimated, but using our model the fate of these "intact" rocks (e.g., impact melt pool) is still predictable.

The large basin impacts dispersed most of the accumulated fragments on their floors, creating "thin spots" in the megaregolith and leaving only their autochthonous fragments (e.g., Imbrium and Orientale basins in Fig. 1e). Comparing the fragment distribution at 3.8 Ga with that at 4.3 Ga, the initial structure of megaregolith caused by the SPA impact is still evident after 0.5 Ga of intensive bombardment, indicating the essential role of the SPA impact on the lunar geology. Due to the great volume of large-scale fragments generated by the SPA impact and their longevity, the seating depth of the large fragments is also closely related to the SPA basin and presents a distinct spatial variation (Fig. 1f). Given that the upper megaregolith is mainly consistent of fragments smaller than 10's of meters, Fig. 1f also indicates that most of the lunar surface is covered with an upper megaregolith thinner than ∼ 5 km being comparable with the recent terrain model (Richardson and Abramov, 2020).

Although the lunar surface is now covered with regolith, the distribution of large fragments in the underlying megaregolith still visibly affects the crater formation. It is, for example, reflected in the distribution of craters with blocky (meter-sized) ejecta that display bright features in Earth-based radar images. Thompson et al. (2009) found that there were about one-third more radar-bright craters north of ∼48°S than to the south over the southeastern nearside highlands (Fig. S3). This suggests that impacts which occurred in the north region are more likely to have excavated big blocks, which agrees with the predicted shallower seating depth of large fragments over the north of the SPA region.

4. Leading factors affecting megaregolith formation

To investigate the leading factors that affect the distribution of megaregolith, simulations with varying settings of fragment distribution are performed. To better compare the results shown in Fig. 1, the sequence of impact craters remains the same. Only the studied parameter is varied, and the values of all the other parameters are identical to those described in Section 2 in each simulation (further details are provided in the supplementary material).

4.1. Model sensitivity

Distribution of Ejected (allochthonous) Fragments The size-frequency distribution of ejected fragments (l_E) and the estimate of the largest fragments (l_{E0}) constrain the distribution of different-sized fragments in ejecta. A steeper slope (the greater b) in l_E indicates a smaller proportion of large fragments. Both experiments and observations of lunar craters suggest b ranging from ∼0.7 to ∼1.8 (Bart and Melosh, 2010; Buhl et al., 2014; Watkins et al., 2019). When a different b is chosen, the fragment size of the surface layer varies. Comparing with the results considering b of 1.2 (Fig. 2a), the layering is identical, but a greater b of 1.8 and a smaller b of 0.7 lead to the decreasing and increasing statistical fragment size of the upper megaregolith by about one and two orders of magnitude, respectively.

Laboratory experiments show an increase of b for impacts into pre-damaged targets (Hartmann, 1969; Ryan et al., 1991) since they generated more abundant small fragments. We conducted simulations considering various b for each impact according to the fragmentation degree of its excavated materials. Since a larger l_V implies generally a more dominant volume of large fragments, for simplicity, we use l_V to represent the relative fragmentation degree. l_V of 1 m (the size of the smallest traced fragments) and ∼15 km (a fragment size indicating intact impact target) relate to the upper and lower limit of b, respectively. The linear relationship between these two end members is used to determine the b value of impacts whose l_V of excavated materials is in between. The results (Fig. 2a) display the identical layering of the upper and lower megaregolith, but the statistical size of fragments in the upper megaregolith falls between that considering a constant b of 0.7 and that considering a constant b of 1.8. In addition, the upper megaregolith itself also shows layering where the fragments in the top ∼500 m are much smaller than the underneath fragments. The small fragments in the near-surface are caused by the repeated occurrence of small impacts. They mostly excavate surface materials that have already been fragmented leading to a greater b and generating abundant small fragments that gather in the near-surface. The deeper fragments exhibit a size closer to the simulation results considering a constant b of 0.7. These fragments are mainly derived from the large-scale basin impacts. Due to their large size, they could easily dig into the deep less damaged crust leading to b near 0.7 and generating abundant large fragments. These large fragments are several kilometers in thickness and only the part in

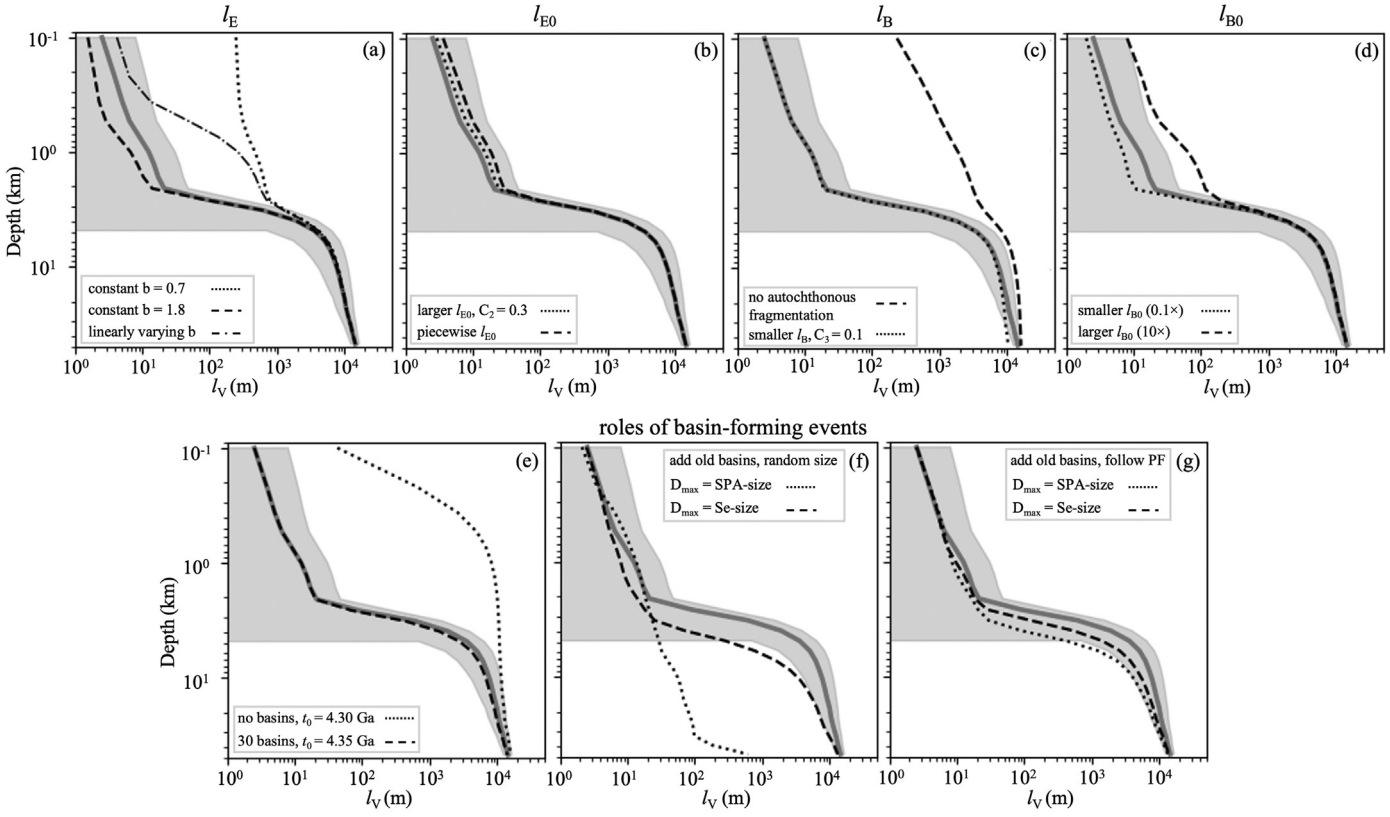

Fig. 2. Influence of varying parameters on the megaregolith formation and the size distribution of fragments. $l_V = \frac{\sum_{i=0}^{14} l_i \times V_i}{\sum_{i=0}^{14} V_i}$ (l_i is the size of fragments and V_i is the volume of fragments with size l_i) is the volume-weighted average fragment size over the surface. The gray solid curves are the estimate based on the assumptions given in Section 2, where the gray areas outline its standard deviation.

the near-surface suffers from the subsequent fragmentation that results in smaller fragments as mentioned above.

In the l_{E0} distribution, observations of lunar craters reveal a C_2 ranging from ~0.1 to ~0.3, which directly affects the calculated size of the largest fragments that deposit near crater rims. In section 3, the value of 0.1 was considered. Simulations with threefold C_2 were run. In addition, the applied l_{E0} distribution was derived from the observations of lunar craters smaller than 100 km. When impact events are large enough, their ejected fragments possess high energy. While emplacing on the surface, they themselves disappear producing secondary craters. Previously, the secondaries were used to constrain the size of the biggest fragments of large-scale impact craters (Allen, 1979; Shoemaker, 1965; Singer et al., 2020 and references therein). Simulations with l_{E0} of craters > 100 km constrained by secondaries were conducted as well (Fig. S2). Both slightly increase the size of the fragments in the upper megaregolith (Fig. 2b), but do not change the predominance of the meter-scale fragments. Although the greater l_{E0} could regionally increase the size of fragments near the crater rims, due to the huge volume of small fragments, the difference of average fragment size becomes small.

Distribution of autochthonous fragments The autochthonous fragmentation process fractures the deep crust resulting in the lower megaregolith (Wiggins et al., 2019). Without this process (Fig. 2c), only the near-surface accumulates some fragments derived from ejecta deposits, the thickness of which is identical as it is mostly generated by the formation of basins which is considered as given. In addition, more large fragments would be generated since most of the impacts can reach the intact crust. Within the crater cavities, the pristine crust would be exposed to space. Both contribute to the greater l_V in the near-surface.

The fragment size of the lower megaregolith depends on the distribution of autochthonous fragments that shows generally increasing size with depth. But autochthonous fragments are so far poorly constrained. Deep drilling of the 40 km Puchezh Katunki impact structure revealed (Ivanov et al., 1996) a generally lower increasing rate (C_3 of 0.1) compared with that from the observation of the 7 km Upheaval Dome crater (C_3 of 0.4, section 3). The slower increasing rate suggests smaller fragments at a certain depth. Simulations with a smaller C_3 of 0.1 (Fig. 2c) show that, despite the regional variation, varying C_3 does not lead to a visible change in the statistical fragment size.

The size of autochthonous fragments close to crater floors (l_{B0}) is constrained by the AF model (Text S1). Given C_3, the potential uncertainty of l_{B0} could affect the size of autochthonous fragments not only seating at the near surface but also at greater depths. Simulations with l_{B0} changed by an order of magnitude (Fig. 2d) showed that the l_V of the upper megaregolith is sensitive to the varying l_{B0} due to its predominance of small-scale fragments, but the l_V of the lower megaregolith barely fluctuates because such difference of l_{B0} is far smaller than the size of its predominant fragments in kilometer-scale.

4.2. Essential role of basin inventory

The large volume of fragments from basin-forming events shapes the structure of megaregolith. Without these giant impacts (Fig. 2e), the accumulated highly fractured crust in the near-surface would be thinner than one kilometer. If the number, location, and timing of basin-forming events is given, the distribution of the upper megaregolith is generally unchanged. However, the distribution of fragments at greater depth could be affected by additional, speculative early basin-forming impact events. In the

simulations above, the crust was assumed to be intact before the SPA formation ($t_0 = 4.3$ Ga). To investigate the influence of the unknown early bombardment history we carried out simulations with an earlier t_0 of 4.35 Ga. We first assume none of these old impacts were of basin-scale. Our results (Fig. 2e) show that the early-formed fragments would be buried to a greater depth leading to a slightly smaller average size of fragments mostly located in a transition zone and the lower megaregolith. Note that impacts that occurred before 4.35 Gyr ago, during the main phase of lunar magma ocean crystallization (Elkins-Tanton et al., 2011), should have failed to produce long-lasting structures.

A more realistic scenario is that during the early bombardment period some number of basins were formed, but any evidence of their existence was erased subsequently. Based on constraints from highly siderophile element abundance in the lunar crust and mantle, Zhu et al. (2019) proposed 90 basins could have been formed between 4.35 to 4.15 Ga, which are 75 basins more than we considered (Fig. 1a). To test the effect of 75 speculative ancient basins between 4.35 and 4.15 Ga we performed additional simulations. As described in section 2, we treat these added basins separately. The basins were randomly distributed over the Moon at random times between 4.15 and 4.35 Ga. Based on the known basin record between 4.35 and 4.15 Ga we estimate the size distribution of the additional basins (the largest SPA basin of 2600 km and the smallest Poincare basin of 312 km). We first consider the randomly assigned size of basins (Fig. 2f). If we keep the uniqueness of the SPA basin and assume there were no erased basins that are larger than the Serenatatis (Se) basin (the observed second largest basin between 4.35 to 4.15 Ga), the SPA basin still displays a major role in the distribution of megaregolith shaping the big picture that is preserved until the present day. If there were many erased basins larger than the Serenatatis basin, the megaregolith would show a distinctly different structure. The statistical size of fragments is then more gently increasing with depth, losing the distinct layer structure. After the cessation time of basin-forming events, the imprint of the SPA event becomes vague. However, this case is highly unlikely because traces of the SPA ejecta manifested in the higher latitude surrounding the SPA cavity are still visible. We then assume the size-frequency distribution of the added basins conforms to the NPF by extrapolating it to the basin size (Fig. 2g, Fig. S4). Because of the shape of the NPF, the number of SPA-sized events is limited. The vertical structure presents comparable layering, although the buried early-formed fragments cause smaller fragments at greater depths. These results further demonstrate that as long as keeping the uniqueness of the SPA basin and absence of other late-forming SPA-sized craters, the megaregolith layering is unchanged and the lateral variation in fragment size is closely related to the deposition of the SPA ejecta.

The incomplete catalog of impact basins and uncertainty regarding their size hamper our knowledge of the early bombardment history of the Moon. Our results suggest that estimating the average thickness of the megaregolith does not allow us to constrain the size-frequency distribution of erased basins. However, the mark they left should be detectable by observations revealing the deep structure. Gravity data from the GRAIL mission yielded insight into the varying thickness of the lunar crust. Positive circular Bouguer anomalies surrounded by negative excursions (inverted sombrero structure) indicate particularly thin crust and uplifted mantle, the typical signatures of basin structures. Based on such gravity data Neumann et al. (2015) added potential structures to lists of lunar basins. The improved basin inventory could be in turn used to constrain the megaregolith distribution.

4.3. Current knowledge of megaregolith distribution

In spite of many uncertainties of parameters concerning the fragment distribution, the 3-layer structure of megaregolith holds. The thickness of each layer is generally constant, the fragment size of each layer is, nevertheless, sensitive to the potential uncertainties. Especially for the fragment distribution of the upper megaregolith, the current empirical knowledge of allochthonous fragments (l_E, l_{E0}) leads to a difference in the average fragments of about two orders of magnitude. The autochthonous fragmentation is the major incentive of the formation of the lower megaregolith. Although this process has been less constrained (l_B, l_{B0}), the dominant fragment size is found to be invariably in kilometer scale. The uncertainty of the basin inventory is another key factor that limits our knowledge of the megaregolith (Hartmann, 2019; Hartmann and Morbidelli, 2020). With the completing of the basin list, especially the old structure-erased ones, the estimated upper megaregolith would increase by several kilometers, and the deep crust of more regions would be damaged by the autochthonous fragmentation.

5. Evolution of megaregolith

Studies of model sensitivities illustrate that, although the potential uncertainties of the applied scaling laws could slightly affect the regional distribution of fragment size, the basin-forming events, as the main drivers of the megaregolith formation, control the evolution of megaregolith. With a given list of basin-forming events, especially those formed after the SPA basin, the distribution of megaregolith is generally unaltered. Fig. 1b shows the distribution of statistical fragment size at different times. The largest SPA-forming event at ~4.3 Ga was the most ancient impact that caused a great volume of fragments. The ejected fragments covered the whole of the Moon forming a kilometer-thick clastic layer, and below its cavity, the fracturing can reach a depth greater than tens of kilometers. In the next 0.2 Ga, the occurrence of multiple basin-forming events that were scattered on the surface shattered more pristine rocks. Their ejected fragments covered the SPA fragments thickening the layer of highly fractured fragments in the near-surface. Beneath their occurrence region, the autochthonous fragmentation process broke the body to greater depths. At 3.9 Ga, when most of the basin-forming events had occurred, the global structure of the megaregolith was established. Due to the thick fragmented layer at the surface, subsequent impact events mostly shattered the generated fragments further, leading to a higher abundance of small fragments. But the late-forming Imbrium and Orientale basins excavated deeper, less damaged crust and emplaced large fragments on the surface, which actually reduced the statistical fragmentation degree of the near-surface (i.e., the larger l_V). Note that, the fracturing depth of large impacts could exceed the thickness of lunar crust and hence the impact-induced megaregolith include not only the crust material but maybe also some upper mantle component. It is consistent with the Apollo seismic data that displays porosity extends to depths up to 15 km below the crust-mantle interface (Lognonné et al., 2003).

The intense growth rate of megaregolith between 4.3 and 4.0 Ga followed by a much lower growth rate is consistent with the estimate from Hartmann (1980, 2019). Based on overturn depths of impact craters, Hartmann estimated the megaregolith evolution as a function of time. The results suggest that given the “accretion tail” impact flux, for a surface formed at 4.3 Ga ago, megaregolith depths of kilometers could easily have accumulated by 4.0 Ga ago. Since then, the megaregolith has been growing much slow and less than 100 m has accumulated until 3.8 Ga.

6. Conclusions

To quantitively constrain the evolution history of the lunar megaregolith and its fragment size, we built a spatially resolved numerical model that considers the processes of both the allochthonous and autochthonous fragmentation. The results underline the predominant role of basin-forming events on the growth of megaregolith. The ancient, large-scale SPA basin shaped the initial structure of the megaregolith. The subsequent impact events regionally alter the megaregolith by either further comminuting the SPA fragments or excavating the less damaged deep crust (and probably some upper mantle), emplacing big fragments near the crater rim. At 3.8 Ga, the megaregolith possesses substantial spatial variation, which is closely related to the distribution of the late-forming impacts, but the big picture of the fragment distribution still displays a close relation to the SPA event.

The megaregolith displays distinct layering with different degrees of fragmentation: The upper megaregolith of ∼2.5 km in thickness mainly consists of meter-scale fragments; the lower megaregolith reaches a depth greater than tens of kilometers and is dominated by kilometer-scale fragments; the transition zone in between mixes fragments of different size scales. The distinct layering may affect the strength and bulk structure of the crust at different depths, which was proposed to affect the dimension of generated craters and hence the shape of crater production function (Marchi et al., 2011). Whether the layering of megaregolith is related to the shape of lunar production function requires more laboratory and numerical experiments and probably some field work and image analysis in the future.

The investigations of the leading factors on the megaregolith formation further demonstrate the essential roles of basin-forming events. The size distribution of allochthonous and autochthonous fragments controls the fragmentation degree of the upper and lower megaregolith, respectively. The uncertainty of the size-frequency distribution (SFD) of allochthonous fragments, which changes the proportion of large fragments, leads to a difference in the fragment size of the upper megaregolith by about two orders of magnitude. More systematic studies on how the SFD of allochthonous fragments changes with impact targets of different damage degrees are required to better constrain the fragment size distribution of highly fractured crust in the near-surface. The uncertainty of the maximum fragments in ejecta would regionally affect the size and the abundance of big fragments near crater rims, but it has a weak effect on the general distribution of different-sized fragments due to the volumetrically predominant role of small fragments. The distribution of the autochthonous fragments has been less constrained. It affects the size of deep-seated fragments, but more importantly, it determines how deep the crust is fractured. More numerical modeling of large-scale impacts could help us better understand the fracturing of the deep crust.

CRediT authorship contribution statement

Tiantian Liu: Conceptualization, Investigation, Methodology, Writing – original draft, Writing – review & editing. **Kai Wünnemann:** Funding acquisition, Methodology, Supervision, Writing – review & editing. **Greg Michael:** Methodology, Writing – review & editing.

Declaration of competing interest

The authors declare that they have no known competing financial interests or personal relationships that could have appeared to influence the work reported in this paper.

Data availability

Data underlie the figures were saved in https://doi.org/10.35003/EBULMM.

Acknowledgements

We greatly appreciate reviews from Bill Hartmann and an anonymous reviewer and the editor for insightful reviews. We acknowledge discussions about fragment distribution and basin inventory with Natalia Artemieva and Robert Luther. We thank Wilhelm Zuschneid for proof-reading. This work was supported by German Research Foundation (DFG) CRC TRR 170, subproject A4. This is TRR 170 Publication No. 175.

Appendix A. Supplementary material

Supplementary material related to this article can be found online at https://doi.org/10.1016/j.epsl.2022.117817.

References

Allen, C.C., 1979. Large lunar secondary craters: size-range relationships. Geophys. Res. Lett. 6, 51–54. https://doi.org/10.1029/GL006i001p00051.
Bart, G.D., Melosh, H.J., 2010. Distributions of boulders ejected from lunar craters. Icarus 209, 337–357.
Besserer, J., Nimmo, F., Wieczorek, M.A., Weber, R.C., Kiefer, W.S., McGovern, P.J., Andrews-Hanna, J.C., Smith, D.E., Zuber, M., 2014. GRAIL gravity constraints on the vertical and lateral density structure of the lunar crust. Geophys. Res. Lett. 41, 5771–5777.
Blanchette-Guertin, J.-F., Johnson, C.L., Lawrence, J.F., 2012. Investigation of scattering in lunar seismic coda. J. Geophys. Res., Planets 117.
Buhl, E., Sommer, F., Poelchau, M.H., Dresen, G., Kenkmann, T., 2014. Ejecta from experimental impact craters: particle size distribution and fragmentation energy. Icarus 237, 131–142.
Elder, C.M., Douglass, B., Ghent, R.R., Hayne, P.O., Williams, J.-P., Bandfield, J.L., Costello, E., 2019. The subsurface coherent rock content of the moon as revealed by cold-spot craters. J. Geophys. Res., Planets 124, 3373–3384.
Elkins-Tanton, L.T., Burgess, S., Yin, Q.Z., 2011. The lunar magma ocean: reconciling the solidification process with lunar petrology and geochronology. Earth Planet. Sci. Lett. 304, 326–336. https://doi.org/10.1016/j.epsl.2011.02.004.
Fassett, C.I., Head, J.W., Kadish, S.J., Mazarico, E., Neumann, G.A., Smith, D.E., Zuber, M.T., 2012. Lunar impact basins: stratigraphy, sequence and ages from superposed impact crater populations measured from Lunar Orbiter Laser Altimeter (LOLA) data. J. Geophys. Res., Planets 117, 1–13. https://doi.org/10.1029/2011JE003951.
Hartmann, W.K., 2019. History of the terminal cataclysm paradigm: epistemology of a planetary bombardment that never (?) happened. Geosciences 9, 285. https://doi.org/10.3390/geosciences9070285.
Hartmann, W.K., 2003. Megaregolith evolution and cratering cataclysm models—lunar cataclysm as a misconception (28 years later). Meteorit. Planet. Sci. 38, 579–593. https://doi.org/10.1111/j.1945-5100.2003.tb00028.x.
Hartmann, W.K., 1980. Dropping stones in magma oceans-effects of early lunar cratering. In: Lunar Highlands Crust, pp. 155–171.
Hartmann, W.K., 1973. Ancient lunar mega-regolith and subsurface structure. Icarus 18, 634–636.
Hartmann, W.K., 1969. Terrestrial, lunar, and interplanetary rock fragmentation. Icarus 10, 201–213. https://doi.org/10.1016/0019-1035(69)90022-0.
Hartmann, W.K., Morbidelli, A., 2020. Effects of early intense bombardment on megaregolith evolution and on lunar (and planetary) surface samples. Meteorit. Planet. Sci. 55, 2472–2492.
Hiesinger, H., 2006. New views of lunar geoscience: an introduction and overview. Rev. Mineral. Geochem. 60, 1–81. https://doi.org/10.2138/rmg.2006.60.1.
Hörz, F., 1977. Impact cratering and regolith dynamics. Phys. Chem. Earth 10, 3–15.
Hörz, F., Grieve, R., Heiken, G., Spudis, P.D., Binder, A., 1991. Lunar surface processes. In: Lunar Sourceb., pp. 61–120.
Housen, K.R., Schmidt, R.M., Holsapple, K.A., 1983. Crater ejecta scaling laws: fundamental forms based on dimensional analysis. J. Geophys. Res., Solid Earth 88, 2485–2499.
Ivanov, B.A., Kocharyan, G.G., Kostuchenko, V.N., Kirjakov, A.F., Pevzner, L.A., 1996. Puchezh-Katunki impact crater: preliminary data on recovered core block structure. In: Lunar and Planetary Science Conference.
Izquierdo, K., Sori, M.M., Soderblom, J.M., Johnson, B.C., Wiggins, S.E., 2021. Lunar megaregolith structure revealed by GRAIL gravity data. Geophys. Res. Lett. 48, e2021GL095978. https://doi.org/10.1029/2021GL095978.

Kenkmann, T., Jahn, A., Wünnemann, K., 2006. "Block size" in a complex impact crater inferred from the upheaval dome structure, Utah. In: 37th Annual Lunar and Planetary Science Conference, p. 1540.

Kenkmann, T., Reimold, W.U., Khirfan, M., Salameh, E., Khoury, H., Konsul, K., 2010. The complex impact crater Jebel Waqf as Suwwan in Jordan: effects of target heterogeneity and impact obliquity on central uplift formation. In: Gibson, R.L., Reimold, Wolf Uwe (Eds.), Large Meteorite Impacts and Planetary Evolution IV. Geological Society of America.

Krishna, N., Kumar, P.S., 2016. Impact spallation processes on the Moon: a case study from the size and shape analysis of ejecta boulders and secondary craters of Censorinus crater. Icarus 264, 274–299. https://doi.org/10.1016/j.icarus.2015.09.033.

Liu, T., Michael, G., Wünnemann, K., Becker, H., Oberst, J., 2020a. Lunar megaregolith mixing by impacts: spatial diffusion of basin melt and its implications for sample interpretation. Icarus 339. https://doi.org/10.1016/j.icarus.2019.113609.

Liu, T., Michael, G., Zhu, M.-H., Wünnemann, K., 2021. Predicted sources of samples returned from chang'e- 5 landing region. Geophys. Res. Lett. 48, e2021GL092434.

Liu, T., Michael, G., Zuschneid, W., Wünnemann, K., Oberst, J., 2020b. Lunar megaregolith mixing by impacts: evaluation of the non-mare component of mare soils. Icarus 114206. https://doi.org/10.1016/j.icarus.2020.114206.

Lognonné, P., Gagnepain-Beyneix, J., Chenet, H., 2003. A new seismic model of the Moon: implications for structure, thermal evolution and formation of the Moon. Earth Planet. Sci. Lett. 211, 27–44. https://doi.org/10.1016/S0012-821X(03)00172-9.

Marchi, S., Massironi, M., Cremonese, G., Martellato, E., Giacomini, L., Prockter, L., 2011. The effects of the target material properties and layering on the crater chronology: the case of Raditladi and Rachmaninoff basins on Mercury. Planet. Space Sci. 59, 1968–1980. https://doi.org/10.1016/j.pss.2011.06.007.

McGetchin, T.R., Settle, M., Head, J.W., 1973. Radial thickness variation in impact crater ejecta: implications for lunar basin deposits. Earth Planet. Sci. Lett. 20, 226–236. https://doi.org/10.1016/0012-821X(73)90162-3.

Melosh, H.J., 1989. Impact Cratering: A Geologic Process. Oxford University, New York.

Melosh, H.J., 1979. Acoustic fluidization: a new geologic process? J. Geophys. Res., Solid Earth 84, 7513–7520.

Melosh, H.J., Ivanov, B.A., 1999. Impact crater collapse. Annu. Rev. Earth Planet. Sci. 27, 385–415.

Moore, H.J., 1970. Large blocks around lunar craters. NASA Spec. Publ. 232, 26.

Neukum, G., 1983. Meteoritenbombardement und Datierung Planetarer Oberflaechen. Habilit. Diss. Fac. Membership, Univ. Munich 1–186.

Neumann, G.A., Zuber, M.T., Wieczorek, M.A., Head, J.W., Baker, D.M.H., Solomon, S.C., Smith, D.E., Lemoine, F.G., Mazarico, E., Sabaka, T.J., Goossens, S.J., Melosh, H.J., Phillips, R.J., Asmar, S.W., Konopliv, A.S., Williams, J.G., Sori, M.M., Soderblom, J.M., Miljković, K., Andrews-Hanna, J.C., Nimmo, F., Kiefer, W.S., 2015. Lunar impact basins revealed by gravity recovery and interior laboratory measurements. Sci. Adv. 1. https://doi.org/10.1126/sciadv.1500852.

Orgel, C., Michael, G., Fassett, C.I., van der Bogert, C.H., Riedel, C., Kneissl, T., Hiesinger, H., 2018. Ancient bombardment of the inner solar system: reinvestigation of the "fingerprints" of different impactor populations on the lunar surface. J. Geophys. Res., Planets 123, 748–762. https://doi.org/10.1002/2017JE005451.

Petro, N.E., Pieters, C.M., 2008. The lunar-wide effects of basin ejecta distribution on the early megaregolith. Meteorit. Planet. Sci. 43, 1517–1529. https://doi.org/10.1111/j.1945-5100.2008.tb01025.x.

Pike, R.J., 1974. Ejecta from large craters on the Moon: comments on the geometric model of McGetchin et al. Earth Planet. Sci. Lett. 23, 265–271. https://doi.org/10.1016/0012-821X(74)90114-9.

Richardson, J.E., Abramov, O., 2020. Modeling the formation of the lunar upper megaregolith layer. Planet. Sci. J. 1, 2.

Rolf, T., Zhu, M.-H., Wuennemann, K., Werner, S.C., 2017. The role of impact bombardment history in lunar evolution. Icarus 286, 138–152.

Ryan, E.V., Hartmann, W.K., Davis, D.R., 1991. Impact experiments 3: catastrophic fragmentation of aggregate targets and relation to asteroids. Icarus 94, 283–298.

Shoemaker, E.M., 1965. Preliminary analysis of the fine structure of the lunar surface in mare cognitum. In: Hess, W.N., Menzel, D.H., O'Keefe, J.A. (Eds.), The Nature of the Lunar Surface, p. 23.

Singer, K.N., Jolliff, B.L., McKinnon, W.B., 2020. Lunar secondary craters and estimated ejecta block sizes reveal a scale-dependent fragmentation trend. J. Geophys. Res., Planets 125, e2019JE006313. https://doi.org/10.1029/2019JE006313.

Thompson, T.W., Campbell, B.A., Ghent, R.R., Hawke, B.R., 2009. Rugged crater ejecta as a guide to megaregolith thickness in the southern nearside of the Moon. Geology 37, 655–658.

Warren, P.H., Rasmussen, K.L., 1987. Megaregolith insulation, internal temperatures, and bulk uranium content of the Moon. J. Geophys. Res., Solid Earth 92, 3453–3465.

Watkins, R.N., Jolliff, B.L., Mistick, K., Fogerty, C., Lawrence, S.J., Singer, K.N., Ghent, R.R., 2019. Boulder distributions around young, small lunar impact craters and implications for regolith production rates and landing site safety. J. Geophys. Res., Planets 124, 2754–2771.

Wieczorek, M.A., Neumann, G.A., Nimmo, F., Kiefer, W.S., Taylor, G.J., Melosh, H.J., Phillips, R.J., Solomon, S.C., Andrews-Hanna, J.C., Asmar, S.W., Konopliv, A.S., Lemoine, F.G., Smith, D.E., Watkins, M.M., Williams, J.G., Zuber, M.T., 2013. The crust of the moon as seen by GRAIL. Science 80 (339), 671–675. https://doi.org/10.1126/science.1231530.

Wiggins, S.E., Johnson, B.C., Bowling, T.J., Melosh, H.J., Silber, E.A., 2019. Impact fragmentation and the development of the deep lunar megaregolith. J. Geophys. Res., Planets 124, 941–957.

Wünnemann, K., Ivanov, B.A., 2003. Numerical modelling of the impact crater depth–diameter dependence in an acoustically fluidized target. Planet. Space Sci. 51, 831–845.

Zhu, M.-H., Artemieva, N., Morbidelli, A., Yin, Q.-Z., Becker, H., Wünnemann, K., 2019. Reconstructing the late-accretion history of the Moon. Nature 571, 226–229. https://doi.org/10.1038/s41586-019-1359-0.